Electronic supplementary information

Co-modification of WO_3 nanoplates with ß-FeOOH/carbon quantum dots combined with plasma treatment enabling high-efficiency photoelectrochemical characteristics

Jui-Teng Lee[a], Zhi-Cheng Yan[a], Kuan-Han Lin[a], Po-Hsuan Hsiao[a], Pin-Chao Liao[b], Ying-Chih Pu[c], and Chia-Yun Chen[a,b,d,e*]

[a]Department of Materials Science and Engineering, National Cheng Kung University, Tainan 70101, Taiwan. *Email: timcychen@mail.ncku.edu.tw

[b]Program on Semiconductor Packaging and Testing, Academy of Innovative Semiconductor and Sustainable Manufacturing, National Cheng Kung University, Tainan 70101, Taiwan.

[c]Department of Materials Science, National University of Tainan, Tainan, 70005, Taiwan.

[d]Program on Smart and Sustainable Manufacturing, Academy of Innovative Semiconductor and Sustainable Manufacturing, National Cheng Kung University, Tainan 70101, Taiwan.

[e]Hierarchical Green-Energy Materials (Hi-GEM) Research Center, National Cheng Kung University, Tainan 701, Taiwan.

*Email: timcychen@mail.ncku.edu.tw

S1 Morphological investigations and correlated band diagram of WO_3-nanoplate based photoanode

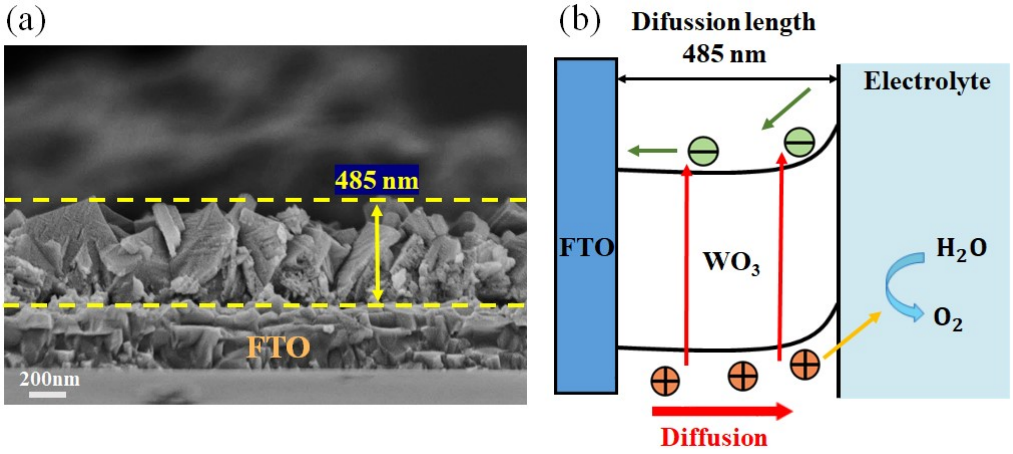

Fig. S1 (a) Cross-section SEM image of WO_3 NPs directly grown on FTO substrate.

(b) Schematic diagram of hole transport across interfaces between WO_3 NPs and electrolytes.

S2 XRD characterizations and LSV measurements of various FeOOH@WO_3 photoanodes

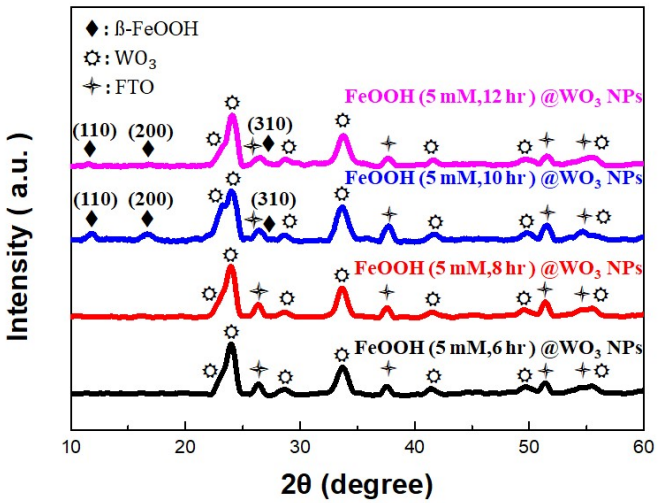

Fig. S2 XRD patterns of prepared β-FeOOH@WO_3 NPs via four various synthetic durations.

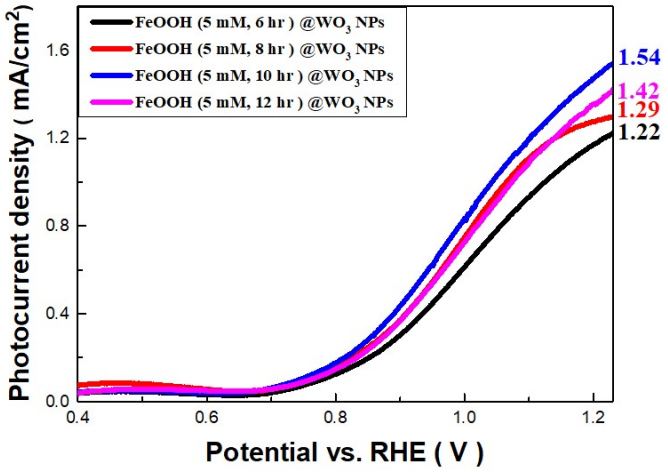

Fig. S3 LSV curves of prepared β-FeOOH@WO_3 NPs via three various synthetic durations. It should be pointed out that the photoanode reported here does not possess the capability to fully split water due to the employment of counter electrode [1-3].

S3 Featuring band diagram of FeOOH@WO_3 NPs with and without undergoing plasma treatment

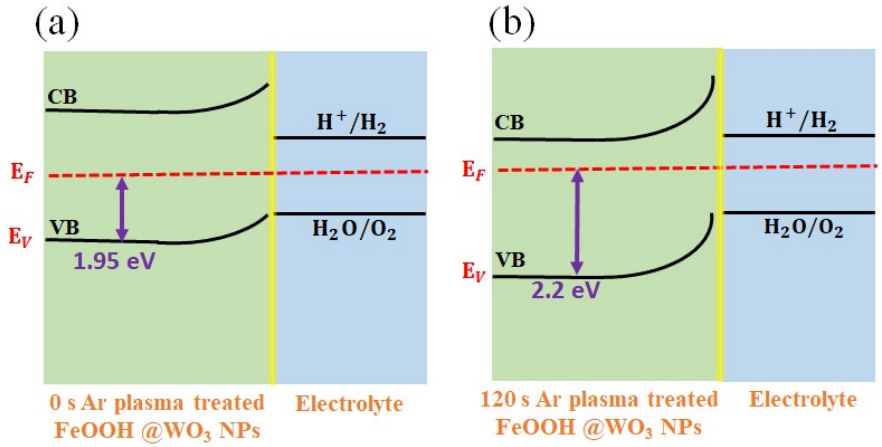

Fig. S4 Schematic illustrations of band diagrams of hybrid FeOOH@WO_3 NPs (a) without plasma treatment and (b) with plasma treatment for 120 s.

S4 Morphological evolutions and chemical compositions of photoanodes under plasma treatment

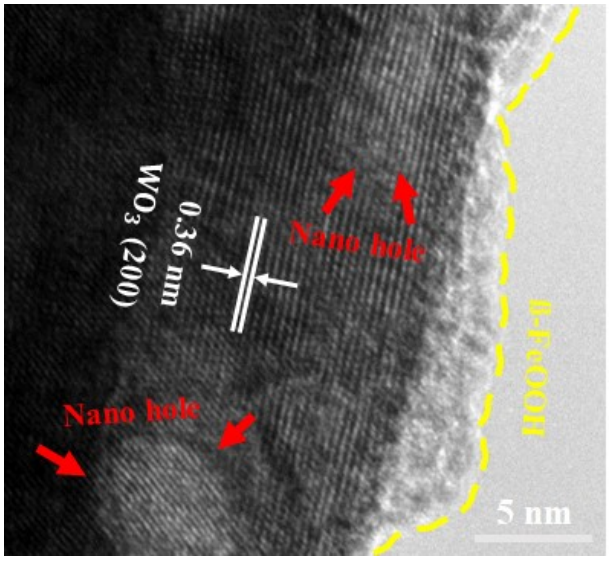

Fig. S5 Representative HRTEM image of p-FeOOH@WO_3 NPs after undergoing 150 s of plasma treatment, where the distorted microstructures are evidenced.

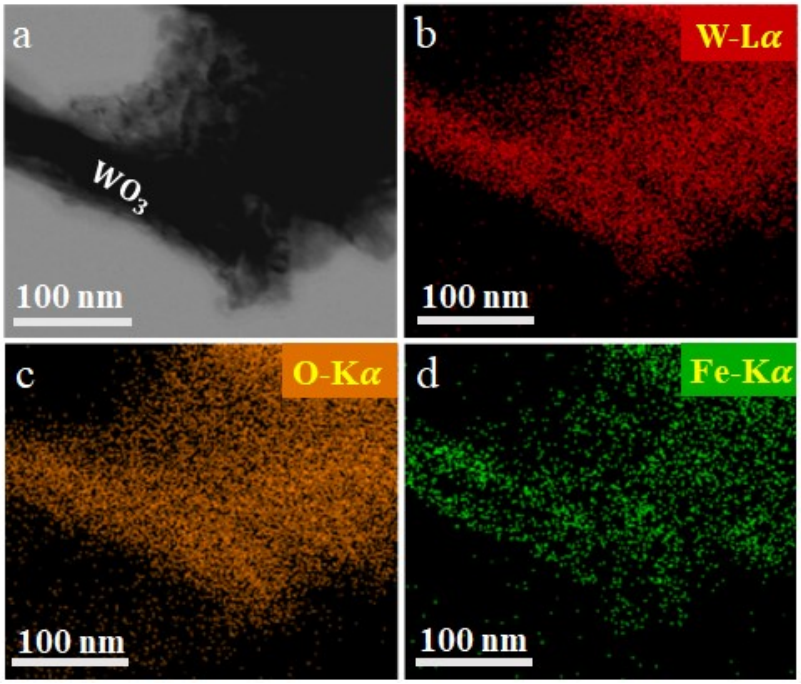

Fig. S6 (a) Representative TEM image of p-FeOOH@WO_3 NPs after undergoing 120 s of plasma treatment, indicating that composite structures are retained without showing distorted features. Corresponding EDS elemental mappings p-FeOOH@WO_3 NPs (120 s) of (b) W element, (c) O element and (d) Fe element, which visualize the uniform compositions of hybrid photoanodes.

S5 Microstructural analysis and size distribution of synthesized CQDs

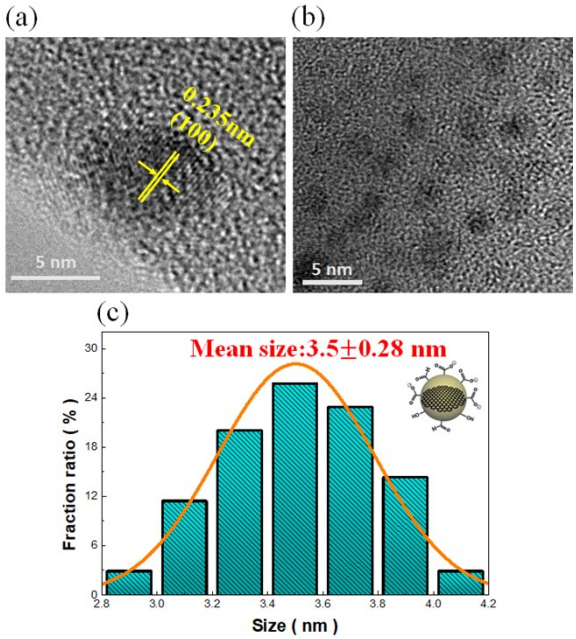

Fig. S7 (a) Representative HRTEM image of a CQD with featured (100) crystallite

fringes. (b) Low magnification TEM image of CQDs, showing the uniform size distributions of obtained CQDs. (c) Estimation of correlated size distributions.

S6 Experimental estimation of band structures

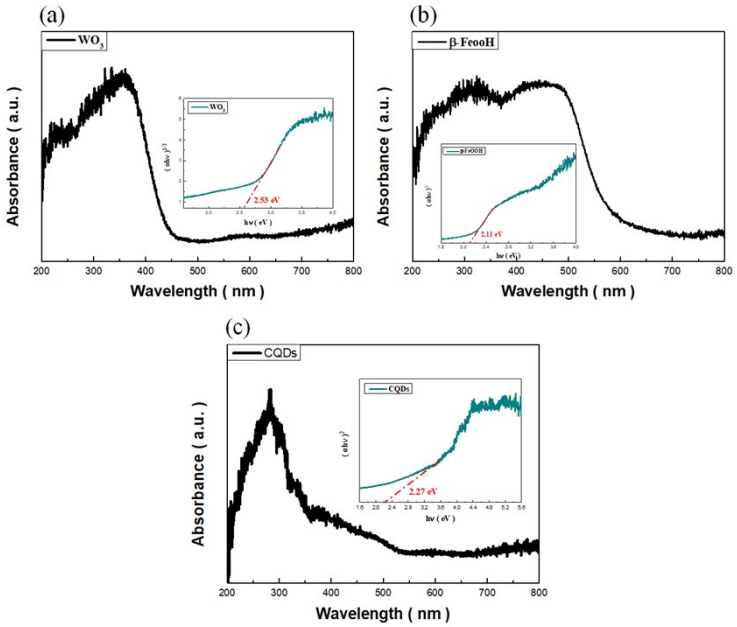

Fig. S8 UV-vis absorption spectra and correlated Tauc examination of (a) bare WO_3 NPs, (b) ß-FeOOH NCs and (c) CQDs.

The analyses of band structures are employed by viture of Tauc plot and UPS measurements. The Tauc plot is obtained by plotting $(\alpha hv)^2$ against hv from UV-Vis absorption spectra, followed by determining the intercept of the tangent line with the X-axis in the Tauc plot to determine the Band gap of the material. Here, α represents the absorption coefficient, h is the Planck constant, and v is the frequency. According to the Tauc plot results, the band gaps of WO_3, β-FeOOH, and CQDs are found to be 2.76 eV, 2.11 eV, and 2.27 eV, respectively. In addition, UPS analysis is employed to estimate the practical position of the valence band using the following formula [4],

$$|VB| = hv - (E_{cutoff} - E_R) \quad (1)$$

where VB the energy level of valence band, ^{hv} the incident photon energy (21.2 eV), $^{E_{cutoff}}$ the energy corresponding to the intersection of extension of vertical line segment and the baseline in the UPS spectrum, ^{E_R} the energy corresponding to the intersection of epitaxial tangent at the initial rise and the baseline. Accordingly, the valence band energies of WO_3, ß-FeOOH, and CQDs are measured to be -7.69 eV, -5.96 eV, and -5.82 eV, respectively.

Table S1. Extracted valence band minimum, conduction band maximum and bandgap energy of investigated structures from the interplay of UPS and UV-Vis light-absorption measurements

	Valence band (eV)	Conduction band (eV)	Band gap (eV)
WO_3	-7.69	-5.16	2.53
β-FeOOH	-5.96	-3.85	2.11
CQDs	-5.82	-3.55	2.27

S7 Analytic XPS spectra of p- FeOOH@WO_3 NPs

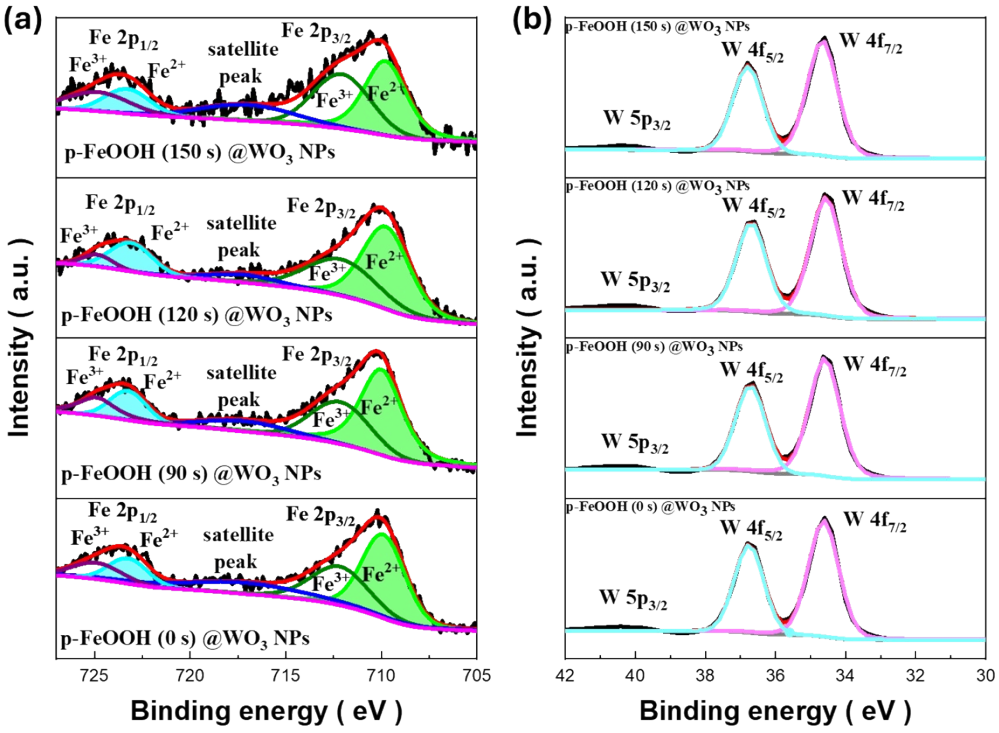

Fig. S9 Analytic XPS spectra of (a) Fe 2p and (b) W 4f for 0 s, 90 s, 120 s, 150 s of p-FeOOH@WO_3 photoanodes. The results from Fe 2p spectra indicate that, under plasma treatment durations of 0, 90, 120, and 150 s, the ratios of Fe^{2+} to Fe^{3+} are observed to be 1.50, 1.61, 1.82, and 1.11, respectively. These findings are in line with the quantitative evolutions shown in Fig. 4 of main text. Furthermore, the results of the W 4f spectra demonstrate the consistent signals of $W4f_{5/2}$, $W4f_{7/2}$, and $W5p_{3/2}$ of samples with or without experiencing the plasma treatment.

S8 Detailed electrochemical CV examinations

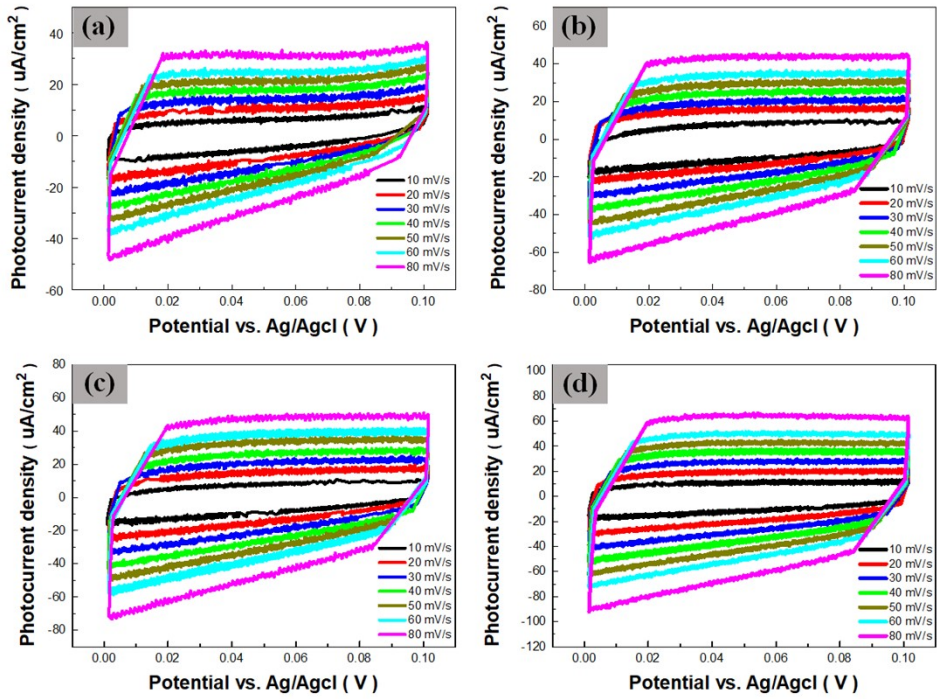

Fig. S10 Electrochemical CV results obtained from the non-Faradic region: (a) Bare WO_3 NPs, (b) FeOOH@WO_3 NPs, (c) p-FeOOH@WO_3 NPs and (d)CQDs/p-FeOOH @WO_3 NPs.

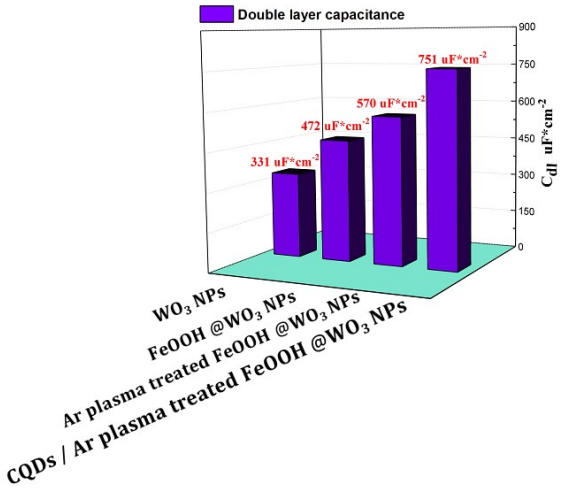

Fig. S11 Comparisons of double layer capacitance (C_{dl}) values from four different photoanode designs.

S9 Faradaic efficiency of O_2 and H_2 production in the presence of designed photoanodes

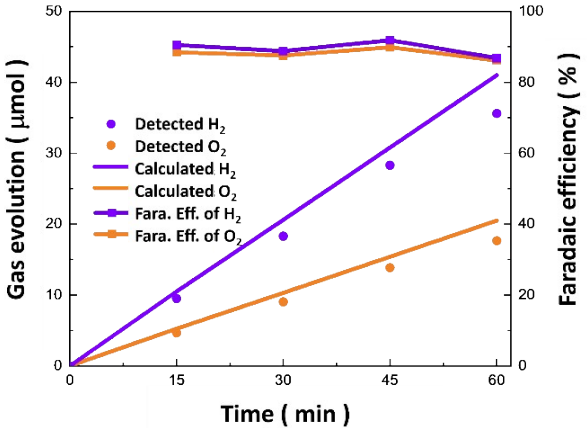

Fig S12 Calculated and measured Faradaic efficiencies at 1.23 V vs. RHE. The results show that after 60 min of water oxidation reaction, the actual yields of hydrogen and oxygen are approximately 35.6 μmol and 17.7 μmol, respectively. In addition, the Faradaic efficiencies for hydrogen and oxygen are estimated to be 89.5% and 88.0%, respectively. highlighting the effectiveness of dual-modification strategies in enhancing water oxidation activity.

S10 Dynamic CV measurement of FeOOH (5 mM)@WO_3 NPs during PEC process

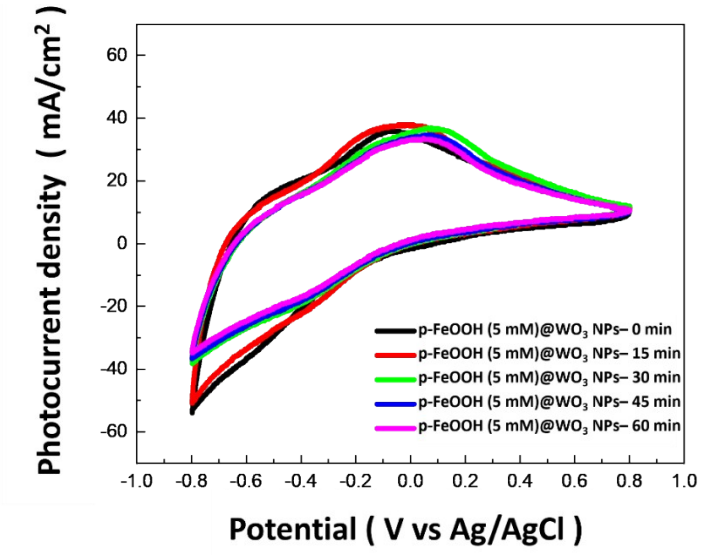

Fig. S13 The dynamic CV measurement of FeOOH (5 mM)@WO_3 NPs during the PEC test. Long-term photoelectrochemical tests of designed photoanodes spanning 0-60 min were conducted [5]. To examine the dynamic changes, the CV results of samples were extracted at every 15 min, with a scan range from 0.8 V to -0.8 V. The results show the consistent oxidation signal at around 0.1 V corresponding to the oxidative conversion of Fe^{2+} states. These findings clearly confirm the existence of Fe^{2+} within electrochemical cycles in all samples.

S11 Morphological characterizations of p-FeOOH@WO_3 NPs after conducting PEC tests

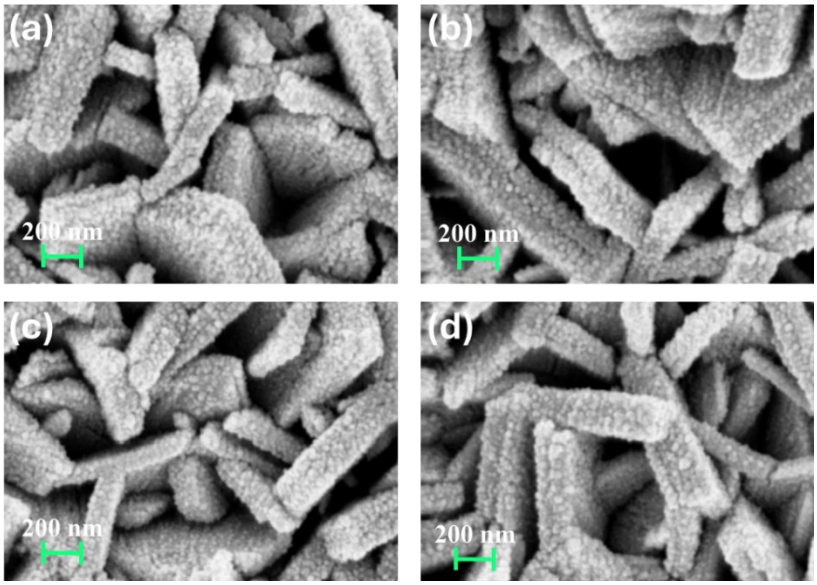

Fig. S14 Top-view SEM images of FeOOH (5 mM)@WO_3 NPs (a) before and (b) after 120 s of Ar plasma treatment. Top-view SEM images of p-FeOOH (5 mM)@WO_3 NPs (120 s of plasma treatment) after experiencing (c) 1-hour and (d) 2-hour photoelectrochemical reactions. The results confirm that no obvious morphological variations of photoanodes after experiencing plasma treatment (120 s) and long-term photoelectrochemical tests.

S12 Mott-Schottky test of FeOOH@WO_3 NPs before and after plasma treatment

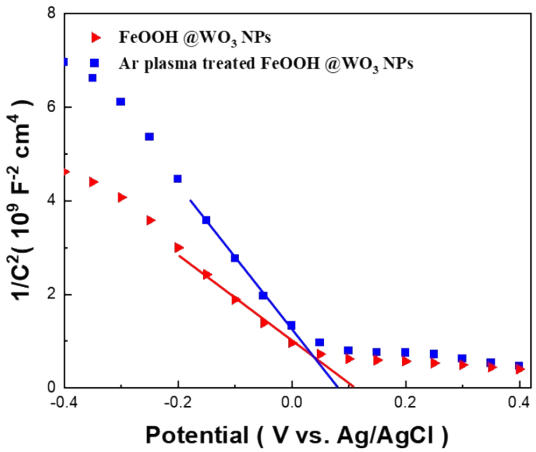

Fig. S15 Measured Mott-Schottky plots of FeOOH@WO_3 NPs before and after Ar plasma treatment. The results indicate that without plasma treatment, the flat band potential of FeOOH@WO_3 NPs at p-type side was measured to be 0.11 V, whereas the

flat band potential of plasma-treated photoanodes was decreased to 0.08 V, suggesting the hole transfer from WO3 NPs to FeOOH that causes the reduction of Fermi level due to p-type doping. Along with photoelectrochemical measurements presented in the main text, these results confirm that the emergence of plasma treatment is effective for inducing band bending at interfaces and facilitates the injection and transport of photogenerated holes.

S13 Stability examinations of p-FeOOH@WO_3 NPs with various treatment durations

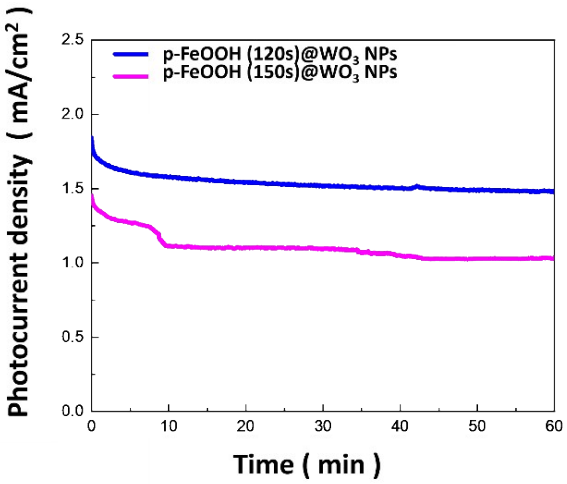

Fig. S16 Stability examinations of photocurrent density versus time in the presence of p-FeOOH @WO_3 photoanode at 1.23 V vs. RHE under the stimulated-light irradiations (100 mW cm^{-2}). The outcomes reveal that the p-FeOOH (120 s)@WO_3 NPs exhibit a stable photocurrent density over an extended period during the stability assessment. In contrast, the photocurrent density of p-FeOOH (150 s)@WO_3 NPs displays significant decrease observed at 8.75 min, indicating that the prolonged plasma treatment may cause the structural degradation of photoanodes. These long-term tests confirm that the emergence of plasma treatment for 120 s represents the optimal solution for both long-term stability and durability.

S14 Comparative table of state-of-art photoanode designs and this work

Table S2 Details of PEC measurements of various photoanode designs

Photoanode materials	**Illumination conditions**	**Eletrolytes**	**Standard photocurrent density**	**Ref**
WO_3/MOS_2	AM 1.5G	0.5 M H_2SO_4	0.96 mA /cm^2 at 1.23 V vs.RHE	[25]
$WO_3/CuWO_4$	500 W X e lamp, $\lambda > 400$ nm	0.2 M Na_2SO_4	1.21 mA /cm^2 at 1.5 V vs.Ag/AgCl	[26]
WO_3/α-Fe_2O_3	300 W Xe lamp, AM 1.5G	0.1 M Na_2SO_4	1 mA /cm^2 at 1.23 V vs.RHE	[27]
$WO_3/BiVO_4$	AM 1.5G	0.5 M Na_2SO_4	1.76 mA /cm^2 at 1.23 V vs.RHE	[28]
WO_3/TiO_2/ NiTCPP	AM 1.5G	0.5 M $NaSO_4$	2.07 mA /cm^2 at 1.23 V vs.RHE	[29]
WO_3/CuO	AM 1.5G	0.5 M Na_2SO_4	1.84 mA /cm^2 at 1.23 V vs.RHE	[32]
$WO_3/ZnWO_4$ /ZnO	500 W Xe lamp	0.35 M Na_2S and 0.25 M $NaSO_3$	1.57 mA /cm^2 at 1.23 V vs.RHE	[50]
WO_3/rGO/Sb_2S_3	AM 1.5G	0.5 M Na_2SO_4	1.20 mA /cm^2 at 1.23 V vs.RHE	[51]
$WO_3/BiVO_4$/ Bi_2S_3	AM 1.5G	0.1 M of Na_2SO_3 and 0.1 M of Na_2S mixed solution	1.52 mA /cm^2 at 1.23 V vs.RHE	[52]
$WO_3/BiVO_4$/ TiO_2	1000 W Xe lamp, AM 1.5G	0.1 M Na_2SO_4	4.2 mA /cm^2 at 1.23 V vs.RHE	[53]
WO_3/PPy:Ru 4POM	300 W Xe lamp	0.1 M HCl	2.5 mA /cm^2 at 1.23 V vs.RHE	[54]
WO_3/C-M2P-CoOx	300 W Xe lamp, AM 1.5G	0.1 M Na_2SO_4	3.5 mA /cm^2 at 1.23 V vs.RHE	[55]
CQDs/p-FeOOH@WO_3	**100 W Xe lamp, AM 1.5G**	**0.1 M Na_2SO_4**	**2.18 mA /cm^2 at 1.23 V vs.RHE** (open-circuit voltage of 0.425 V)	**This work**

Reference

1. Lopes, P. Dias, L. Andrade and A. Mendes, *Solar Energy Materials and Solar Cells*, 2014, **128**, 399-410.
2. S.S. Kalanur, I.-H. Yoo, K. Eom and H. Seo, *Journal of Catalysis*, 2018, **357**, 127-137.
3. Y. Zhao, S. Balasubramanyam, R. Sinha, R. Lavrijsen, M.A. Verheijen, A.A. Bol and A. Bieberle-Hütter, *ACS Applied Energy Materials*, 2018, **1**, 5887-5895.
4. H.W. Du, J. Yang, Y.H. Li, F. Xu, J. Xu and Z.Q. Ma, *Applied Physics Letters* 2015, **106**, 093508.
5. H. Ma, Y. Zheng, J. Xian, Z. Feng, Z. Li and F. Cui, *Chemosphere*, 2022, **296**, 133994.